Estimation of the chiral magnetic effect considering the magnetic field response of the QGP medium [*]

Sheng-Qin Feng(冯笙琴)[1,2,3;1]   Xin Ai(艾鑫)[1]   Lei Pei(裴蕾)[1]   Fei Sun(孙飞)[1]

Yang Zhong(钟洋)[1]   Zhong-Bao Yin(殷中宝)[2]

[1] College of Science, China Three Gorges University, Yichang 443002, China
[2] Key Laboratory of Quark and Lepton Physics (MOE) and Institute of Particle Physics,
Central China Normal University, Wuhan 430079, China
[3] School of Physics and Technology, Wuhan University, Wuhan 430072, China

Abstract: The magnetic field plays a major role in searching for the chiral magnetic effect in relativistic heavy-ion collisions. If the lifetime of the magnetic field is too short, as predicted by simulations of the field in vacuum, the chiral magnetic effect will be largely suppressed. However, the lifetime of the magnetic field will become longer when the QGP medium response is considered. We give an estimate of the effect, especially considering the magnetic field response of the QGP medium, and compare it with the experimental results for the background-subtracted correlator H at RHIC and LHC energies. The results show that our method explains the experimental results better at the top RHIC energy than at the LHC energy.

1   Introduction

The interplay of quantum anomalies and magnetic fields leads to a lot of macroscopic quantum phenomena in relativistic heavy-ion collisions. The most important one, which we discuss here, is the chiral magnetic effect (CME). The CME is the separation of electric charge along the magnetic field in the presence of chirality imbalance [1–3]. It has already been observed in condensed matter systems [4].

The question is whether the CME exists in relativistic heavy-ion collisions. The answer seems to be yes. Two necessary conditions, chirality imbalance and magnetic field, may be met in QGP produced in relativistic heavy-ion collisions. Firstly, quantum chromodynamics (QCD), which describes the behavior of the QGP, permits topological charge changing transitions that can induce chirality imbalance [1]. Secondly, an enormous magnetic field can be produced in non-central relativistic heavy-ion collisions due to charged nuclei moving at speeds close to the speed of light [5–10]. Therefore, the CME is very likely to exist in relativistic heavy-ion collisions.

Over the past few years, much effort has been given to the search for experimental evidence of the CME in relativistic heavy-ion collisions. Several collaborations at the BNL Relativistic Heavy Ion Collider (RHIC), and the CERN Large Hadron Collider (LHC), including STAR [11–17], PHENIX [18], and ALICE [19, 20] have studied this; for recent reviews see Ref. [21].

At first glance, it seems easy to detect the CME experimentally. In fact, this is not the case. Firstly, one cannot identify the charge asymmetry in an individual event as a sign of the CME. This is due to the fact that statistical fluctuations $\sim \sqrt{N}$ are much larger than the expected charge asymmetry induced by the CME, where N is the charged-particle multiplicity of produced particles [1]. However, if one directly takes an average over many events, the contributions of the CME will also be canceled out, since right-handed and left-handed chirality is produced with equal probability.

One proposal is to measure the charge separation fluctuations perpendicular to the reaction plane by a three-point correlator, $\gamma \equiv \langle\langle\cos(\phi_\alpha+\phi_\beta-2\Psi_{\mathrm{RP}})\rangle\rangle$, where the averaging is done over all particles in an event and over all events [1, 22]. This correlator will remove the multiplicity fluctuations while keeping the contributions from the CME. The γ correlator was first measured by the STAR Collaboration for Au+Au and Cu+Cu collisions at 62.4 and 200 GeV [11, 12]. All the results have

been found to be qualitatively consistent with the theoretical expectation of the CME. Similar results have also been observed by the ALICE Collaboration for 2.76 TeV Pb+Pb collisions [20].

Unfortunately, the γ correlator still contains some background contributions not related to the CME [23–25]. These background contributions are mainly from the elliptic flow in combination with two-particle correlations. To solve this problem, the two-particle correlator, $\delta \equiv \langle \cos(\phi_\alpha - \phi_\beta) \rangle$, is introduced. Similar to the γ correlator, δ also contains the contributions from the CME and the backgrounds, but it is dominated by backgrounds. It is suggestive to express γ and δ in the following ways [25, 26]:

$$\gamma = \kappa v_2 B - H, \tag{1}$$

$$\delta = B + H, \tag{2}$$

where H and B are the CME and background contributions, respectively. The background-subtracted correlator, H, can be obtained by solving Eqs. (1) and (2):

$$H^\kappa = \frac{\kappa v_2 \delta - \gamma}{1 + \kappa v_2}. \tag{3}$$

The coefficient κ is close to but deviates from unity owing to the finite detector acceptance and theoretical uncertainties [25]. The δ correlators for 200 GeV Au+Au collisions and 2.76 TeV Pb-Pb collisions have been measured by STAR [12] and ALICE [20], respectively. The correlator $H_{SS} - H_{OS}$ has been measured by STAR for Au+Au collisions at $\sqrt{s_{NN}} = 7.7$–62.4 GeV [16]. The results show that there is a clear charge-separation effect at $\sqrt{s_{NN}} = 19.6$–200 GeV for mid-peripheral (30%–80% centrality) collisions. This is again in line with the expectations for the CME.

To better explain the experimental results, a quantitative estimation of the CME is needed. In Ref. [1], Kharzeev, McLerran, and Warringa (KMW) developed a quantitative model to estimate the CME-induced charge separation.

One of the main issues in estimating the CME is the time evolution of the magnetic field in relativistic heavy-ion collisions. This issue has been studied in many works [1, 5–10]. The numerical calculations carried out in these studies show that an enormous magnetic field ($B \sim 10^{15}$ T) can be found at the very beginning of the collisions. However, according to these studies, the strength of the magnetic field decreases rapidly with time. This is a challenge for the manifestation of the CME in relativistic heavy-ion collisions. If the lifetime of the magnetic field is too short, the imprint of the CME might be negligible. Nevertheless, it has been proposed that these estimations of the magnetic field are valid only in the early stage of the collision. Later, the magnetic response from the QGP medium becomes increasingly

important [8, 9, 27–33], and the magnetic field will be maintained for a much longer time than in the vacuum.

This work aims to give an estimation of the CME, especially considering the magnetic response of the QGP medium, and then compare it with the experimental results for the background-subtracted correlator H.

This paper is organized as follows. We give an introduction of the KMW model in Section 2. The time evolution of the magnetic field in relativistic heavy-ion collisions is discussed in Section 3. In Section 4, we present our computation results, and a summary is given in Section 5.

2   KMW model for the CME

In this section, we will briefly introduce the KMW model for estimating the CME in relativistic heavy-ion collisions.

All gauge field configurations which have finite action can be categorized into topologically distinct classes labeled by the winding number Q_w. Configurations with non-zero Q_w can induce chirality imbalance through the axial anomaly. If initially there are an equal number of right-handed and left-handed fermions, i.e., $N_R = N_L$, at $t = \infty$ we have

$$(N_L - N_R)_{t=\infty} = 2N_f Q_w. \tag{4}$$

The classical vacuum of QCD is degenerate, and the winding number n_w can characterize the different classical vacua. It can be shown that if a gauge field configuration with non-zero Q_w goes to a pure gauge at infinity, it induces a transition from one classical vacuum to another.

The transition can be achieved through an instanton [34, 35] or sphaleron [36, 37]. The instanton corresponds to quantum tunneling through the energy barrier between different QCD vacua, which is highly suppressed. However, the sphaleron corresponds to going over the barrier, and its transition rate can be very high at high temperature, which happens to be the situation for QGP. Thus, it provides the chance to induce chirality.

The transition rate for the QCD has been estimated in Ref. [1] as follows:

$$\frac{\mathrm{d}N_t^\pm}{\mathrm{d}^3x \mathrm{d}t} \equiv \Gamma^\pm \sim 192.8\alpha_S^5 T^4, \tag{5}$$

where the superscript $\pm$ denotes the transitions with $Q_w = \pm 1$. The total rate of transition is the sum of the rates of the lowering and rising transition,

$$\frac{\mathrm{d}N_t}{\mathrm{d}^3x \mathrm{d}t} = \sum_\pm \frac{\mathrm{d}N_t^\pm}{\mathrm{d}^3x \mathrm{d}t}. \tag{6}$$

In the case of a sufficiently large magnetic field, the charge separation parallel to the magnetic field induced

by a configuration with winding number Q_w is as follows,

$$Q = 2Q_w \sum_f |q_f|, \qquad (7)$$

where q_f is the charge in units of e of a quark with flavor f. For a moderate magnetic field, the estimation given by Ref. [1] is

$$Q \approx 2Q_w \sum_f |q_f| \gamma(2|q_f \Phi|), \qquad (8)$$

where

$$\gamma(x) = \begin{cases} x, & \text{for } x \leqslant 1, \\ 1, & \text{for } x \geqslant 1, \end{cases} \qquad (9)$$

and $\Phi = eB\rho^2$ is the flux through a configuration of size ρ with non-zero Q_w.

Now we consider the situation in relativistic heavy-ion collisions. We use the same symbols defined in Ref. [1]. $N_a^\pm$ and $N_b^\pm$ denote the total positive/negative charge in units of e above (a) and below (b) the reaction plane respectively; $\Delta_\pm$ is the difference in charge between each side of the reaction plane $\Delta_\pm = N_a^\pm - N_b^\pm$.

When there is a transition from one vacuum to another, a charge difference will be created locally. However, the quarks may encounter many interactions in the QGP, and this will suppress the degree of the final observed charge separation. In considering this, the screening suppression functions $\xi_\pm(x_\perp)$ are introduced in Ref. [1]. The expression is as follows,

$$\xi_\pm(x_\perp) = \exp(-|y_\pm(x) - y|/\lambda), \qquad (10)$$

where λ is the screening length and $y_\pm(x)$ is the upper and lower y coordinate of the overlap region. The expectation value of the change of the Δ_+ and Δ_- due to a transition is either positive or negative with equal probability and given by

$$\pm \sum_f |q_f| \gamma(2|q_f \Phi|) \xi_\pm(x_\perp). \qquad (11)$$

Here only the most probable transitions have been considered, namely $Q_w = \pm 1$.

By assuming that all transitions happen independently from each other, one can compute the variation of $\Delta^\pm$:

$$\langle \Delta_\pm^2 \rangle = \frac{1}{2} \int_{t_i}^{t_f} dt \int_V d^3x \int d\rho \frac{dN_t}{d^3x dt d\rho}$$
$$\times [\xi_-(x_\perp)^2 + \xi_+(x_\perp)^2] \Big[\sum_f |q_f| \gamma(2|q_f eB|\rho^2) \Big]^2, \qquad (12)$$

and $\langle \Delta_+ \Delta_- \rangle$ can also be calculated:

$$\langle \Delta_+ \Delta_- \rangle = - \int_{t_i}^{t_f} dt \int_V d^3x \int d\rho \frac{dN_t}{d^3x dt d\rho}$$
$$\times \xi_-(x_\perp) \xi_+(x_\perp) \Big[\sum_f |q_f| \gamma(2|q_f eB|\rho^2) \Big]^2. \qquad (13)$$

In Ref. [1], Eqs. (12) and (13) have been rewritten for small magnetic fields $(2|q_f eB| < 1/\rho^2)$ using Eq. (5) for transition rate and the fact that $\rho \sim (\Gamma^\pm/\alpha_S)^{-1/4} \sim 1/(\alpha_S T)$. They are given as follows,

$$\frac{d\langle \Delta_\pm^2 \rangle}{d\eta} = 2\kappa \alpha_S \Big[\sum_f q_f^2 \Big]^2 \int_{V_\perp} d[2]x_\perp$$
$$\times [\xi_-(x_\perp)^2 + \xi_+(x_\perp)^2] \int_{\tau_i}^{\tau_f} d\tau \tau [eB(\tau, \eta, x_\perp)]^2, \qquad (14)$$

$$\frac{d\langle \Delta_+ \Delta_- \rangle}{d\eta} = -4\kappa \alpha_S \Big[\sum_f q_f^2 \Big]^2 \int_{V_\perp} d[2]x_\perp$$
$$\times \xi_+(x_\perp) \xi_-(x_\perp) \int_{\tau_i}^{\tau_f} d\tau \tau [eB(\tau, \eta, x_\perp)]^2, \qquad (15)$$

where the proper time $\tau = (t^2 - z^2)^{1/2}$ and the space-time rapidity $\eta = \frac{1}{2} \log[(t+z)/(t-z)]$. The volume integral is over the overlap region $V_\perp$ in the transverse plane. The assumption here is that the magnetic field does not change the transition rate dramatically. There is also a constant κ for which the order of magnitude should be one, but with large uncertainties [1].

In Ref. [1], $\langle \Delta_\pm^2 \rangle$ and $\langle \Delta_+ \Delta_- \rangle$ are connected to the correlators $a_{++}(a_{+-})$ by the expressions

$$a_{++} = a_{--} = \frac{1}{N_+^2} \frac{\pi^2}{16} \langle \Delta_\pm^2 \rangle, \qquad (16)$$

$$a_{+-} = \frac{1}{N_+ N_-} \frac{\pi^2}{16} \langle \Delta_+ \Delta_- \rangle, \qquad (17)$$

where $N_\pm$ is the total number of positively or negatively charged particles in the corresponding η interval. The correlator $a_{++}(a_{+-})$ is the same as the γ correlator, except for a sign difference. However, in this model the v_2-related backgrounds are completely ignored; thus we should compare the model-calculated correlators $a_{++}(a_{+-})$ with the background-subtracted correlator $H_{SS}(H_{OS})$. Because H also has a sign difference with γ as shown in Eq. (1), there is no sign difference between $a_{++}(a_{+-})$ and $H_{SS}(H_{OS})$.

3 Magnetic field in relativistic heavy-ion collisions

We will discuss the magnetic field in relativistic heavy-ion collisions in this section. Reference [1] gave a calculation of the magnetic field in relativistic heavy-ion

collisions. The calculation was done by an analytic model with the assumption that the nucleon density is uniform in the rest frame. On this basis, Ref. [10] improved the calculation by using the Woods-Saxon nucleon distribution. There are also many other calculations using different methods [5–9].

However, most of these calculations did not consider the magnetic response of the QGP medium, which may significantly influence the time evolution of the magnetic field. Tuchin first analyzed it in Refs. [27, 28], and he concluded that the magnetic field is almost constant during the entire plasma lifetime due to high electric conductivity. Later, it was quantitatively studied in many works [8, 9, 29–33]. To explore this problem, one needs to consider the electric conductivity σ and chiral magnetic conductivity σ_χ which is induced by the CME. In Ref. [29], it was found that the effects of finite σ_χ are not important for the top RHIC and LHC energies. Therefore, we do not consider the effects of chiral magnetic conductivity in this paper. For the electric conductivity σ, there are a lot of theoretical uncertainties [38–41].

For computational simplicity, we adopt the most optimistic situation proposed in Ref. [8], namely assuming the electric conductivity σ is large enough that we can take the QGP as an ideally conducting plasma. Under this assumption, one gets the following equations from Maxwell's equations:

$$\frac{\partial \boldsymbol{B}}{\partial t} = \nabla \times (\boldsymbol{v} \times \boldsymbol{B}), \qquad (18)$$

$$\boldsymbol{E} = -\boldsymbol{v} \times \boldsymbol{B}, \qquad (19)$$

where the $\boldsymbol{v}$ is the flow velocity of QGP.

To solve the above equations, one needs to know the evolution of $\boldsymbol{v}$. In Ref. [8], the Bjorken picture was assumed for the longitudinal expansion,

$$v_z = \frac{z}{t}. \qquad (20)$$

For transverse expansion, a linearized ideal hydrodynamic equation proposed by Ref. [42] was applied, giving the following solution,

$$v_x = \frac{c_s^2}{a_x^2} x t, \qquad (21)$$

$$v_y = \frac{c_s^2}{a_y^2} y t, \qquad (22)$$

where c_s is the speed of sound, and $a_{x,y}$ is the root-mean-square of the transverse entropy distribution. Here, we take $a_x \sim a_y \sim 3$ and $c_s^2 \sim 1/3$.

Substituting the velocity into Eqs. (18)-(19), one can solve $\boldsymbol{B}(t)$ for a given initial condition $\boldsymbol{B}^0(\boldsymbol{r}) = \boldsymbol{B}(t = t_0, \boldsymbol{r})$ where t_0 is the formation time of the QGP. Here, we only consider the y component of the magnetic field at the center of the collision region, and get the following

solution,

$$B_y(t, \boldsymbol{0}) = \frac{t_0}{t} \mathrm{e}^{-\frac{c_s^2}{2a_x^2}(t^2 - t_0^2)} B_y^0(\boldsymbol{0}). \qquad (23)$$

To get the time evolution of magnetic field from Eq. (23), we must know the formation time t_0 of the QGP and the initial magnetic field at that time, namely $B_y^0(\boldsymbol{0})$. For initial magnetic field, we use the method in Ref. [10], which does not consider the QGP medium response. For the formation time of the QGP, the following approximation formula has been used:

$$t_0 \sim 1/Q_s, \qquad (24)$$

where Q_s is the saturation momentum.

The value of saturation momentum Q_s for Au-Au collisions at $\sqrt{s} = 130$ GeV is provided by Ref. [43]. We use the following formula for estimating the energy and nuclear dependence of the saturation momentum [44]:

$$Q_s^2 \sim A^{1/3} x^{-0.3}, \qquad (25)$$

where Bjorken $x = Q_s / \sqrt{s}$. Then, the saturation momentum for collisions with different nuclei and center-of-mass energy can be calculated by the results of Ref. [43] using Eq. (25).

The centrality dependence of Q_s^2, t_0, and eB_y^0 for Au-Au collisions at RHIC energy and Pb-Pb collisions at LHC energy have been given in Tables 1–2, where the average impact parameter b is inferred from Refs. [45, 46]. The time evolution of magnetic field is plotted in Fig. 1, and the magnetic field in vacuum is also added for comparison.

Table 1.   Centrality dependence of Q_s^2, t_0 and eB_y^0 for Au-Au collisions at $\sqrt{s} = 200$ GeV.

centrality(%)	b/fm	Q_s^2/GeV^2	t_0/fm	eB_y^0/MeV^2
0–5	2.21	2.25	0.132	2161.4
5–10	4.03	2.15	0.135	3382.9
10–20	5.70	1.99	0.140	3942.6
20–30	7.37	1.75	0.149	3909.5
30–40	8.73	1.50	0.161	3447.2
40–50	9.90	1.22	0.179	2771.0
50–60	11.00	0.92	0.205	2001.3

Table 2.   Centrality dependence of Q_s^2, t_0 and eB_y^0 for Pb-Pb collisions at $\sqrt{s} = 2760$ GeV.

centrality(%)	b/fm	Q_s^2/GeV^2	t_0/fm	eB_y^0/MeV^2
0–5	2.43	4.52	0.093	700.8
5–10	4.31	4.33	0.095	782.8
10–20	6.05	4.01	0.099	673.4
20–30	7.81	3.53	0.105	469.3
30–40	9.23	3.01	0.114	287.0
40–50	10.47	2.45	0.126	151.1
50–60	11.58	1.86	0.145	64.5

We also compare our results with those of McLerran & Skokov [29] and Tuchin [30, 33], which are plotted in Fig. 2. In Fig. 2(a), we compare with McLerran &

Skokov's results for Au-Au collisions at $\sqrt{s}=200$ GeV and $b=6$ fm. The solid line represents our method; the dash-dotted line represents McLerran & Skokov's results in the vacuum; and the dotted line represents McLerran & Skokov's results with the conductivity set by lattice QCD calculation.
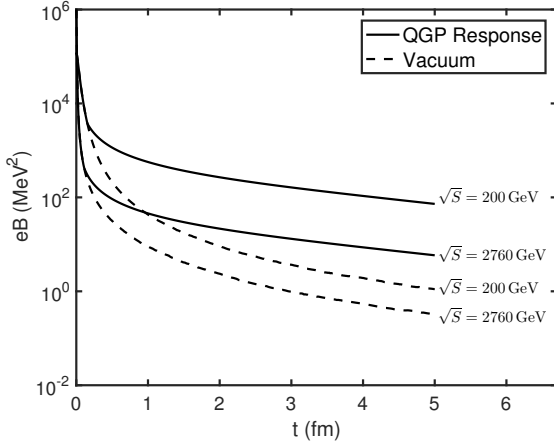

Fig. 1.   Time evolution of magnetic field for Au-Au collisions with $b=8$ fm at $\sqrt{s}=200$ GeV and Pb-Pb collisions with $b=8$ fm at $\sqrt{s}=2760$ GeV. The solid line and dashed line represent the results with and without considering the QGP medium, respectively.
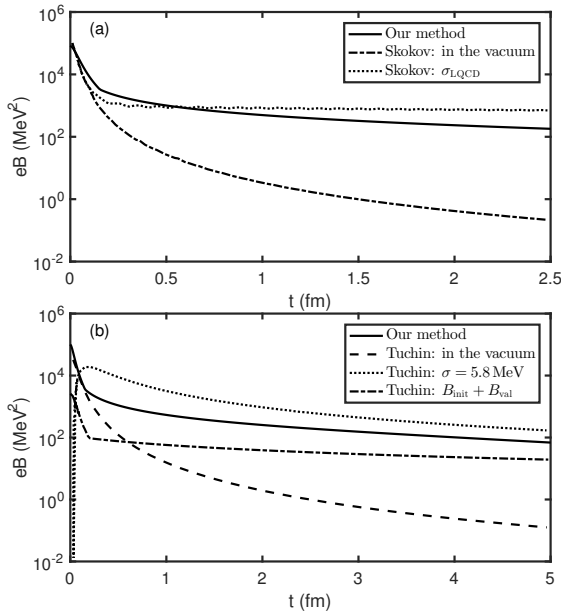

Fig. 2.   Comparison of our results with those of McLerran & Skokov [29] (a) and Tuchin [30, 33] (b).

We find that McLerran & Skokov's magnetic field drops more rapidly than ours in the beginning, and it

goes down more slowly at later times. Possible causes of the difference are the different settings in electric conductivity σ, and the neglect of the influence of flow velocity $\boldsymbol{v}$ and QGP formation time t_0 by McLerran & Skokov.

In Fig. 2(b), we compare with Tuchin's results for Au-Au collisions at $\sqrt{s}=200$ GeV and $b=7$ fm. The solid line represents our method, and the dashed line represents Tuchin's result in the vacuum. The dotted line represents Tuchin's result by setting electric conductivity $\sigma=5.8$ MeV [30]. However, Ref. [30] did not consider the contributions from the initial magnetic field and also ignored the QGP formation time t_0. This explains why the magnetic field increases rapidly from zero at the beginning. The result of considering the initial magnetic field [33] is plotted by the dash-dotted line in Fig. 2(b) with the QGP formation time $t_0=0.2$ fm. Reference [33] simplified relativistic heavy-ion collisions as two counter-propagating charges, which may be the main reason for the difference in magnitude from our result. Nevertheless, the overall trend of our result is very similar to that of Ref. [33].

4   Computation results

In this section, we are going to give an estimation of the CME in relativistic heavy-ion collisions using the KMW model introduced in Section 2.

We use Eqs. (14)–(17) to determine the centrality dependence of the correlator $a_{++}(a_{+-})$. The time evolution of magnetic field has been discussed in Section 3. For the correspondence between impact parameter and centrality, we refer to Refs. [45, 46]. The number of charged particles $N_{\pm}$ is obtained from Refs. [45, 47]. As explained in Section 1, the KMW model does not consider the contributions from the background, so we compare our results with the experimental results for the background-subtracted correlator H. The undetermined parameters χ and λ are fixed by fitting the experiment observable $H_{\mathrm{SS}}-H_{\mathrm{OS}}$. The results for Au-Au collisions at $\sqrt{s}=200$ GeV and Pb-Pb collisions at $\sqrt{s}=2760$ GeV are plotted in Fig. 3.

It can be seen from Fig. 3 that the model explains the experimental data better at RHIC than LHC energy. For Au-Au collisions at $\sqrt{s}=200$ GeV, the general trend is consistent with experiment, but it deviates from experiment for peripheral collisions. This may be due to the hard-sphere approximation which is used in determining the overlap region $V_{\perp}$ in Eq. (14) and Eq. (15).

For Pb-Pb collisions at $\sqrt{s}=2760$ GeV, it rises as centrality goes up (more peripheral) for central collisions and then falls for peripheral collisions. This trend is completely different from the experimental data. The reasons for its fall for peripheral collisions are as follows. In general, the magnetic field in vacuum increases with

increasing impact parameter b. However, the magnetic field considering QGP medium has a strong dependence on QGP formation time t_0 at high energy. As we can see from Fig. 1, the magnetic field drops more quickly at high energy. Therefore, a slight change in t_0 will greatly influence the magnetic field and then the CME. Besides, from Tables 1–2 we know that t_0 becomes larger for peripheral collisions. The combination of these leads to the fall of the correlator $a_{++}-a_{+-}$ in peripheral collisions. This effect also exists in Au-Au collisions at $\sqrt{s}=200$ GeV, but it is weaker at low energy.
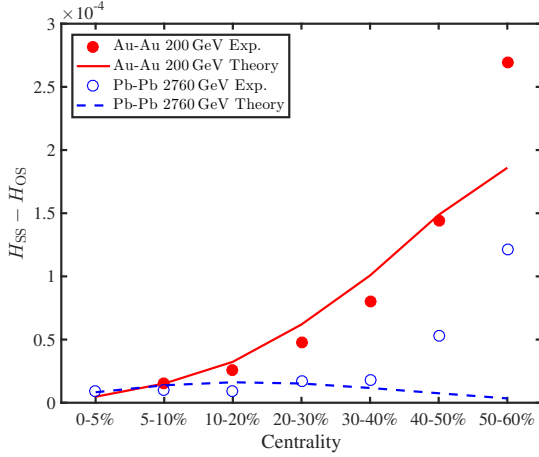

Fig. 3.   (color online) Comparison between the centrality dependence of $a_{++}-a_{+-}$ estimated with the KMW model and the background-subtracted experiment observable $H_{\mathrm{SS}}-H_{\mathrm{OS}}$.

This discrepancy between theory and experiment at high energy reflects the shortcomings of our model. This may be because we only consider the magnetic field at the origin, namely $B_y(t,\mathbf{0})$, for simplicity. It is appropriate when the magnetic field is homogeneous. At high energy, however, the magnetic field may be highly inhomogeneous in the beam direction. Therefore, only considering the magnetic field at the origin will greatly underestimate the overall effects. This problem should be further studied in later works.

Generally, the correlator a_{+-} is less than a_{++} because of the screening effect. We plot the centrality dependence of $|a_{+-}|/a_{++}$ with different screening lengths for Au-Au collisions at $\sqrt{s}=200$ GeV in Fig. 4. The results are similar to the results in Ref. [1]: the correlator $|a_{+-}|/a_{++}$ increases as impact parameter b increases. This is because the system size is small when the impact parameter b is large, and the smaller the system size, the weaker the screening effect. Note that the weaker the screening effect, the bigger the correlator $|a_{+-}|/a_{++}$ and when there is no screening effect, the correlator $|a_{+-}|/a_{++}$ should be equal to 1. This also explains why the correlator $|a_{+-}|/a_{++}$ increases as screening length λ increases.

The experimental data for the δ correlator for Cu-Cu collisions is absent, so we cannot get its background-subtracted correlator H. Therefore, we estimated the correlator $a_{++}-a_{+-}$ for Cu-Cu collisions at $\sqrt{s}=200$ GeV using the same parameter settings from Au-Au collisions. The results are plotted in Fig. 5. The results for Au-Au collisions at $\sqrt{s}=200$ GeV are also plotted in Fig. 5 for comparison. As can be seen from the figure, the correlator for Au-Au collisions is much larger than that for Cu-Cu collisions.
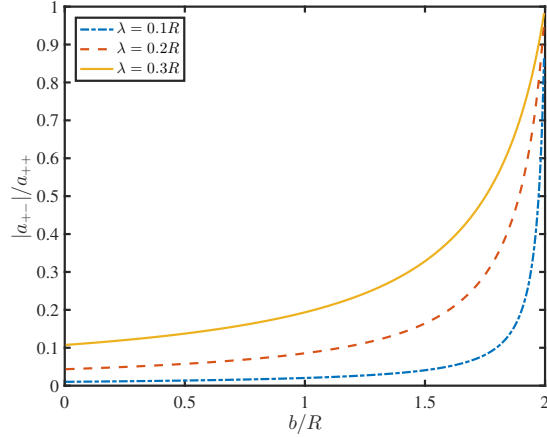

Fig. 4.   (color online) Results for the correlator $|a_{+-}|/a_{++}$ as a function of b/R with different screening lengths λ for Au-Au collisions at $\sqrt{s}=200$ GeV.
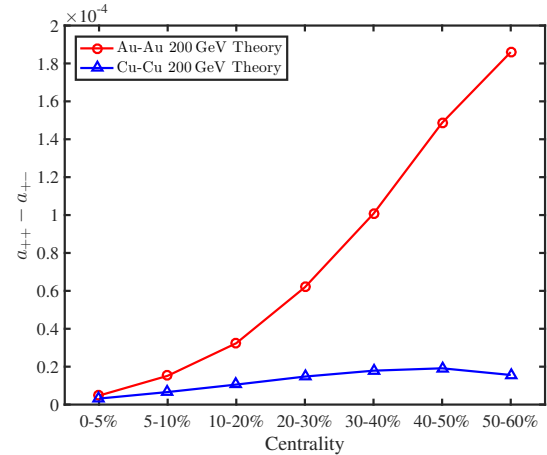

Fig. 5.   (color online) Estimation of the correlator $a_{++}-a_{+-}$ for Cu-Cu collisions at $\sqrt{s}=200$ GeV.

The main reason for this result is that, at the same centrality, the smaller the system size, the smaller the initial magnetic field. To illustrate this point, we present the centrality dependence of Q_{s}^2, t_0, and eB_y^0 for Cu-Cu collisions at $\sqrt{s}=200$ GeV in Table 3. Comparing Table 1 and Table 3, we find that the initial magnetic field of Cu-Cu collisions is 3 to 5 times lower than that of Au-Au collisions.

Table 3.   Centrality dependence of Q_s^2, t_0 and eB_y^0 for Cu-Cu collisions at $\sqrt{s}$=200 GeV.

centrality(%)	b/fm	Q_s^2/GeV^2	t_0/fm	eB_y^0/MeV^2
0–5	1.75	1.62	0.155	619.7
5–10	2.80	1.55	0.159	782.5
10–20	3.97	1.43	0.165	818.5
20–30	5.15	1.26	0.176	728.9
30–40	6.10	1.07	0.191	590.5
40–50	6.92	0.88	0.211	446.0
50–60	7.68	0.66	0.242	311.4

5   Summary

In this paper, we have estimated the CME in relativistic heavy-ion collisions considering the magnetic field response of the QGP medium. The QGP medium has a significant influence on the time evolution of the magnetic field.   To estimate the magnetic field, we adopted the optimistic assumption that the electric conductivity σ of the medium is large enough to take QGP as an ideally conducting plasma. The time evolution of the magnetic field is substituted into the KMW model to estimate the CME in relativistic heavy-ion collisions.

We compared our calculation results with the experimental results for the background-subtracted correlator H. The results show that our method explains the experimental data better for RHIC than for the LHC. The failure of our method for the LHC results may be due to the assumption that the magnetic field is homogeneously distributed in space, which is not satisfied at the LHC. The specific explanation remains to be studied further. The centrality dependence of the correlator $|a_{+-}|/a_{++}$ for different screening lengths was presented, and the results are similar to those of Ref. [1]. Finally, we gave an estimation of the correlator a_{++}–a_{+-} for Cu-Cu collisions at RHIC energy and find it is much smaller than that of Au-Au collisions with the same energy and centrality.

References

1 D. E. Kharzeev, L. D. McLerran, and H. J. Warringa, Nucl. Phys. A, **803**: 227–253 (2008)
2 H. J. Warringa, J. Phys. G, **35**: 104012 (2008)
3 K. Fukushima, D. E. Kharzeev, and H. J. Warringa, Phys. Rev. D, **78**: 074033 (2008)
4 Q. Li, D. E. Kharzeev, C. Zhang et al, Nature Phys., **12**: 550–554 (2016)
5 V. V. Skokov, A. Yu. Illarionov, and V. D. Toneev, Int. J. Mod. Phys. A, **24**: 5925–5932 (2009)
6 V. Voronyuk, V. D. Toneev, W. Cassing et al, Phys. Rev. C, **83**: 054911 (2011)
7 A. Bzdak and V. Skokov, Phys. Lett. B, **710**: 171–174 (2012)
8 W. T. Deng and X. G. Huang, Phys. Rev. C, **85**: 044907 (2012)
9 K. Tuchin, Phys. Rev. C, **88**: 024911 (2013)
10 Y. J. Mo, S. Q. Feng, and Y. F. Shi, Phys. Rev. C, **88**: 024901 (2013)
11 B. I. Abelev et al, Phys. Rev. Lett., **103**: 251601 (2009)
12 B. I. Abelev et al, Phys. Rev. C, **81**: 054908 (2010)
13 S. A. Voloshin et al, Indian J. Phys., **85**: 1103–1107 (2011)
14 L. Adamczyk et al, Phys. Rev. C, **88**: 064911 (2013)
15 G. Wang, Nucl. Phys. A, **904-905**: 248c–255c (2013)
16 L. Adamczyk et al, Phys. Rev. Lett., **113**: 052302 (2014)
17 L. Adamczyk et al, Phys. Rev. C, **89**: 044908 (2014)
18 N. N. Ajitanand, S. Esumi, and R. A. Lacey, in: Proc. of the RBRC Workshops, **96** (2010)
19 P. Christakoglou, J. Phys. G, **38**: 124165 (2011)
20 B. Abelev et al, Phys. Rev. Lett., **110**: 012301 (2013)
21 G. Wang, L. Wen, Adv. High Energy Phys., **2017**: 9240170 (2017)
22 S. A. Voloshin, Phys. Rev. C, **70**: 057901 (2004)
23 S. Schlichting and S. Pratt, Phys. Rev. C, **83**: 014913 (2011)
24 S. Pratt, S. Schlichting, and S. Gavin, Phys. Rev. C, **84**: 024909 (2011)
25 A. Bzdak, V. Koch, and J. Liao, Lect. Notes Phys., **871**: 503–536 (2013)
26 J. Liao, Pramana, **84**: 901 (2015)
27 K. Tuchin, Phys. Rev. C, **82**: 034904 (2010)
28 K. Tuchin, Phys. Rev. C, **83**: 039903 (2011)
29 L. McLerran and V. Skokov, Nucl. Phys. A, **929**: 184–190 (2014)
30 K. Tuchin, Adv. High Energy Phys., **2013**: 490495 (2013)
31 B. G. Zakharov, Phys. Lett. B, **737**: 262–266 (2014)
32 K. Tuchin, Phys. Rev. C, **91**: 064902 (2015)
33 K. Tuchin, Phys. Rev. C, **93**: 014905 (2016)
34 D. Diakonov, Prog. Part. Nucl. Phys., **51**: 173–222 (2003)
35 T. Schäfer and E. V. Shuryak, Phys. Rev. D, **53**: 6522–6542 (1996)
36 P. B. Arnold and L. D. McLerran, Phys. Rev. D, **37**: 1020 (1988)
37 M. Fukugita and T. Yanagida, Phys. Rev. D, **42**: 1285–1286 (1990)
38 P. B. Arnold, G. D. Moore, and L. G. Yaffe, JHEP, **05**: 051 (2003)
39 S. Gupta, Phys. Lett. B, **597**: 57–62 (2004)
40 H. T. Ding, A. Francis, O. Kaczmarek et al, Phys. Rev. D, **83**: 034504 (2011)
41 A. Francis and O. Kaczmarek, Prog. Part. Nucl. Phys., **67**: 212–217 (2012)
42 J.-Y. Ollitrault, Eur. J. Phys., **29**: 275–302 (2008)
43 D. Kharzeev and M. Nardi, Phys. Lett. B, **507**: 121–128 (2001)
44 H. Kowalski, T. Lappi, and R. Venugopalan, Phys. Rev. Lett., **100**: 022303 (2008)
45 R. L. Ray and M. Daugherity, J. Phys. G, **35**: 125106 (2008)
46 B. Abelev et al, Phys. Rev. C, **88**: 044909 (2013)
47 K. Aamodt et al, Phys. Rev. Lett., **106**: 032301 (2011)